Charge Tuning of Nonresonant Magnetoexciton Phonon Interactions in Graphene

Sebastian Rémi,[1] Bennett B. Goldberg,[1,2,3] and Anna K. Swan[2,1,3,*]
[1]Boston University, Department of Physics, 590 Commonwealth Avenue, Boston, Massachusetts 02215, USA
[2]Boston University, Department of Electrical and Computer Engineering, Boston, Massachusetts 02215, USA
[3]Boston University, Photonics Center, 8 St. Mary's St, Boston, Massachusetts 02215, USA
(Received 23 July 2013; published 7 February 2014)

Far from resonance, the coupling of the G-band phonon to magnetoexcitons in single layer graphene displays kinks and splittings versus filling factor that are well described by Pauli blocking and unblocking of inter- and intra-Landau level transitions. We explore the nonresonant electron-phonon coupling by high-magnetic field Raman scattering while electrostatic tuning of the carrier density controls the filling factor. We show qualitative and quantitative agreement between spectra and a linearized model of electron-phonon interactions in magnetic fields. The splitting is caused by dichroism of left- and right-handed circular polarized light due to lifting of the G-band phonon degeneracy, and the piecewise linear slopes are caused by the linear occupancy of sequential Landau levels versus ν.

DOI: 10.1103/PhysRevLett.112.056803 PACS numbers: 73.22.Pr, 63.22.Rc, 71.70.Di, 81.05.ue

When Dirac fermions in graphene are subjected to a perpendicular magnetic field B, the electronic states form discrete, degenerate Landau levels (LLs) with energy of $E_{\pm,n} = \pm v_F\sqrt{2e\hbar Bn}$ (n is the Landau level index) [1,2]. Each level has spin(2) and valley(2) degeneracy with a system occupancy described by the filling factor $\nu = h\tilde{n}/eB$, where $\tilde{n}$ is the surface density of charges [3]. At charge neutrality $\nu = 0$ and the $n = 0$ level is half filled.

Superpositions of inter-LL magnetoexcitons and optical phonons show a resonance in the magnetophonon response when the energy of an allowed LL transition matches the phonon energy [2–5]. Systems where the electronic and phonon dephasing is smaller than the electron-phonon interaction strength show pronounced anticrossings of the energy of the coupled phonon magnetoexciton states. Anticrossings at resonance have been observed by magneto-Raman spectroscopy of decoupled surface layers of graphene on graphite [6–8] and more recently on exfoliated graphene on SiO_2 [9]. In cases without full coherence, the phonon energy is still shifted by the enhanced electron phonon coupling near resonances as has been observed on multilayer graphene on SiC [10], graphite [11,12], and graphene on SiO_2 [13].

Magnetoexciton transitions couple to orthogonal states of the degenerate modes of the G-band phonon. Symmetry allowed transitions obey the selection rule $\Delta|n| = \pm 1$ [11]. Experimentally selective excitation of the orthogonal states is achieved using cross circular polarized optical excitation and detection channels. In a σ^+/σ^- configuration, only states coupling to $\Delta n = +1$ transitions can be observed, while only states coupling to $\Delta n = -1$ transitions are observed in σ^-/σ^+ polarization configuration [6,9,11,13]. These selection rules create optical dichroism for doped graphene [3,4] and have been observed in graphene on SiO_2 due to partial Pauli blocking of the initial or final Landau level states [9,13]. High quality graphene on SiC or on graphite can be considered charge neutral, while exfoliated graphene on SiO_2 typically shows accidental doping from sample preparation and impurities in the substrate. So far, only limited control of the doping level $\tilde{n}$ has been achieved by annealing and gas exposure in between scanned B-field measurements [9]. However, for constant $\tilde{n}$ the filling factor ν varies with the B-field strength. We use graphene field effect devices, widely used in transport [14–16] as well as Raman measurements [17–19], to provide full control of the charge density and decouple the effects of magnetic field and filling factor dependence.

Here we show for the first time charge carrier density dependent magneto-Raman measurements on single layer graphene field effect devices at constant magnetic fields. Contrary to previous magnetophonon studies, we explore the Raman response in a magnetic field far from magnetophonon resonance conditions. We demonstrate a linear dependence with ν for the nonresonant regime, rather than the $\sqrt{\nu}$ behavior predicted for the on-resonance response. Notably, at constant magnetic field we observe pronounced splittings and slope changes of the G-band phonon energy as a function of ν, the LL filling. We show that the structure in the electron-phonon coupling is due to the occupancy of Landau level magnetoexciton transitions coupled to the phonon. In contrast to on-resonance measurements, no single transition dominates the coupling, and several inter- and intraband transitions have to be considered to account for the experimental observations. Splitting is due to the different filling factor dependent response to left- and right-hand polarized light.

For control of the charge carrier density we fabricated field effect devices based on single layer graphene where

the charge density is controlled by the gate voltage. Graphene is exfoliated onto a 300 nm thick SiO_2/Si substrate and the devices are fabricated using standard microfabrication processes. We confirm the single layer character by Raman spectroscopy and measurement of the optical contrast [20–23].

Raman measurements are performed at 4 K in a He bath cryostat, schematically drawn in Fig. 1(a). The sample is mounted on a piezoelectric x-y-z stage at the focus of a confocal, free-space microscope cooled with He exchange gas and placed in the center of a superconducting magnet with an accessible range of $B = \{0T, 12.6T\}$. The Raman response is excited using a HeNe Laser at $\lambda = 632.8$ nm with a diffraction limited spot size ~ 1 μm. The excitation laser is linearly polarized, although we do not monitor or optimize the polarization. Since our experiment uses linear polarized light without an analyzer, we measure both σ^+/σ^- and σ^-/σ^+ transitions; i.e., both $\Delta|n| = \pm 1$ transitions are detected simultaneously. Scattered light is filtered by a long pass filter to remove the laser light, collected by a single mode fiber and analyzed using a conventional grating spectrometer.

Figure 1(b) illustrates the effect of applying a backgate voltage V_{bg} at finite magnetic field of $B = 12.6$ T. For $\nu = -4.7$ ($V_{bg} = -20$ V) the G band is symmetric with a single peak (black line), but splits into 2 peaks for $\nu = -1.8$ ($V_{bg} = -8$ V) due to the interaction of the optical phonons with the discrete Landau levels [24].

Characterization of the phonon response versus charge density was performed by Raman spectroscopy while sweeping the backgate in the range $V_{bg} = \{-40\text{ V}, 40\text{ V}\}$ both at $B = 0$ T as well as $B = 12.6$ T. Figure 2 shows a Raman intensity map of the observed spectra as a function of V_{bg}. We extract the position of the G band by fitting the spectra with single ($B = 0$ T) and double Lorentzian ($B = 12.6$ T) functions shown in Figs. 2(c) and (d).

Measurement results at $B = 0T$ are shown in Figs. 2(a) and (c). The behavior of the G band as a function of charge density has previously been studied theoretically and experimentally [17–19,25]. We use the model of Ref. [25] to fit the data, and also include the effects of inhomogeneous broadening due to charge carrier density fluctuations [18]. In Fig. 2(c) we plot the fit results (red dashed line) as a function of V_{bg}, and extract the following system parameters: The electron-phonon coupling strength $\lambda = (4.5 \pm 0.5) \times 10^{-3}$, the phenomenological broadening parameter [25] $\delta = 10$ meV, the unperturbed phonon energy at $B = 0$ T, $\varepsilon = 1582.0$ cm^{-1}, the inhomogeneous broadening $\delta\tilde{n} = 0.3 \times 10^{12}$ cm^{-2} (standard deviation of a Gaussian distribution), and finally the Fermi velocity $v_F = (1.10 \pm 0.1) \times 10^6$ ms^{-1}. The extracted values of Fermi velocity v_F and λ agree well with those determined in previous experiments on SiO_2 [9,13]. However, for graphene on graphite, a lower v_F, and a 23% higher value of λ is reported [8]. For more details on the qualitative and quantitative analysis at $B = 0$ T we refer to the Supplemental Material [26].

Figures 2(b) and 2(d) show a very different behavior for $B = 12.6$ T. G-band splitting starts around $\nu = -6$ ($V_{bg} \approx -25$ V) then reaches a maximum at $\nu = -2$ ($V_{bg} \approx -9$ V), disappears at $\nu = 0$ ($V_{bg} = 0$ V), and repeats symmetrically for $\nu > 0$. The largest magnitude of the splitting is ~ 12 cm^{-1}. At $B = 12.6$ T, the nearest magnetophonon resonances are the transitions between

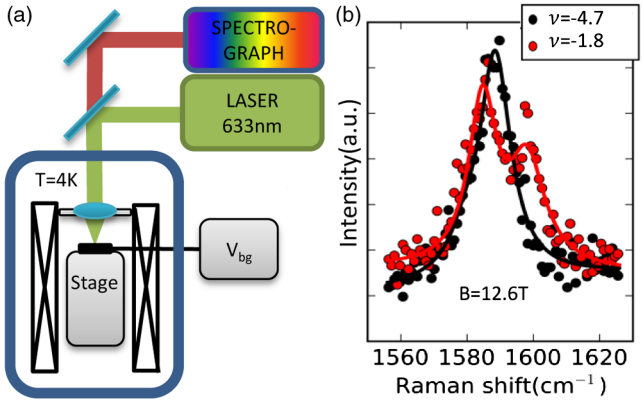

FIG. 1 (color online). (a) Schematic view of the cryogenic Raman setup using linearly polarized light. (b) G-band Raman spectra at $B = 12.6$ T. Black spectrum measured at $\nu = -4.7$ ($V_{bg} = -20$ V). The red spectrum shows visible splitting of the G band at $\nu = -1.8$ ($V_{bg} = -8$ V). Solid lines are double-peaked Lorentzian fits.

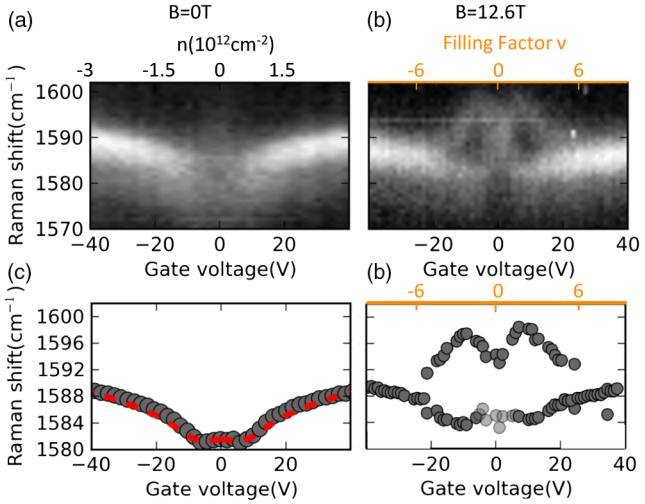

FIG. 2 (color online). Raman intensity map of the G-band Raman spectra as a function of applied backgate voltage. The charge density and filling factor are indicated on top of the figures. (a) Measurements for $B = 0$ T. (b) $B = 12.6$ T. A clear splitting is visible for voltages $|V| \leq 20$V. (c) and (d) show phonon energies from Lorentzian fits in (a) and (b). Dashed red line is a fit using a model of the phonon anomaly in graphene [25]. Light grey points are due to a weak asymmetry in the peak visible for low intensity (see Supplemental Material [26]).

$|n| = 0$ and $|n| = 1$ at $B = 25\ T$ and $|n| = 1$ and $|n| = 2$ at $B = 4.1\ T$.

Following Refs. [3,4,13] we consider the phonon energy $\varepsilon_{\mathcal{A}}$ in Eq. (1). The index $\mathcal{A}$ denotes the two orthogonal circularly polarized phonon states accessed by σ^+ or σ^- circularly polarized light.

$$\varepsilon_{\mathcal{A}}^2 - \varepsilon_0^2 = 2\varepsilon_0\lambda T_0^2\left[\sum_{n=0}^{N}\left(\frac{f_{\mathcal{A},n}(\nu)T_n}{(\varepsilon_{\mathcal{A}}+i\delta)^2 - T_n^2} + \frac{1}{T_n}\right) + \sum_{n=1}^{N}\frac{f_{\mathcal{A},n}(\nu)S_n}{(\varepsilon_{\mathcal{A}}+i\delta)^2 - S_n^2}\right] \quad (1)$$

Here ε_0 is the unperturbed phonon energy, λ is the dimensionless electron-phonon coupling parameter, and δ is the phenomenological broadening introduced by Ando [4]. The two sums are the contribution from all the interband and intraband asymmetric transitions [see Fig. 3(a)]. The interband transitions have energy $T_n = T_0(\sqrt{n+1} + \sqrt{n})$ and intraband transitions $S_n = T_0(\sqrt{n+1} - \sqrt{n})$ where $T_0 = v_F\sqrt{2e\hbar B}$. For $B = 12.6\ T$, $T_0 \approx 140$ meV compared with $\sim$196 meV for the G band phonon. The filling factor dependence of the coupling to the highly degenerate Landau level states is described by the factor $f_{\mathcal{A},n}$. For interband transitions $f_{\mathcal{A},n}$ is defined by

$$f_{\sigma^+,n} = (1+\delta_{n,0})(\bar{\nu}_{-n} - \bar{\nu}_{+(n+1)})$$
$$f_{\sigma^-,n} = (1+\delta_{n,0})(\bar{\nu}_{-(n+1)} - \bar{\nu}_{+n}). \quad (2)$$

Here $\bar{\nu}_n$ is the normalized filling factor describing the fraction of filling of the nth Landau level. It is related to the filling factor ν by $\bar{\nu}_{\pm n} = [\nu - (4(\pm n) - 2)]/4$ since each Landau level state is fourfold degenerate. Hence $0 < \bar{\nu}_n < 1$. The definition of $f_{\mathcal{A},n}$ for intraband transition is easily obtained by replacing the index $\mp n$ by $\pm n$. In Fig. 3(a) we illustrate the level occupation for a filling factor $\nu = 2$; i.e., the $n = 0$ level is completely filled (partial filling factor $\bar{\nu}_0 = 1$). Hence, the transition between $n = -1$ and $n = 0$ is Pauli blocked (dashed lines in figure) and $f_{\sigma^-,0} = 0$, while all transitions originating from the $n = 0$ level have maximum strength due to the high density of occupied states that can be excited, with $f_{\sigma^+,0} = 1$.

Equation (1) is valid for all B fields and charge states, although it is cumbersome to use. Near resonance, a single resonant term dominates, so other terms can be neglected in solving Eq. (1). The solution is described by a two-level coupled mode model [8,9]

$$\varepsilon_{\mathcal{A}}^{\pm} = \frac{T_n + \varepsilon_0}{2} \pm \sqrt{\left(\frac{T_n - \varepsilon_0}{2}\right)^2 + \frac{\lambda T_0^2}{2} f_{\mathcal{A},n}}. \quad (3)$$

Equation (3) describes the anticrossing between the coherent coupled states $\varepsilon_{\mathcal{A}}^{\pm}$. The index $\pm$ refers to the upper and lower branches of the anticrossing.

In the nonresonant regime, where our experiment is performed, the approximation leading to Eq. (3) is not valid. Since $\Delta\varepsilon_{\mathcal{A}} = \varepsilon_{\mathcal{A}} - \varepsilon_0$ is small, Eq. (1) can be linearized by noting that $\varepsilon_{\mathcal{A}}^2 - \varepsilon_0^2 \approx (\varepsilon_{\mathcal{A}} - \varepsilon_0)2\varepsilon_0$, and replacing the $\varepsilon_{\mathcal{A}}$ in the denominator by the unperturbed

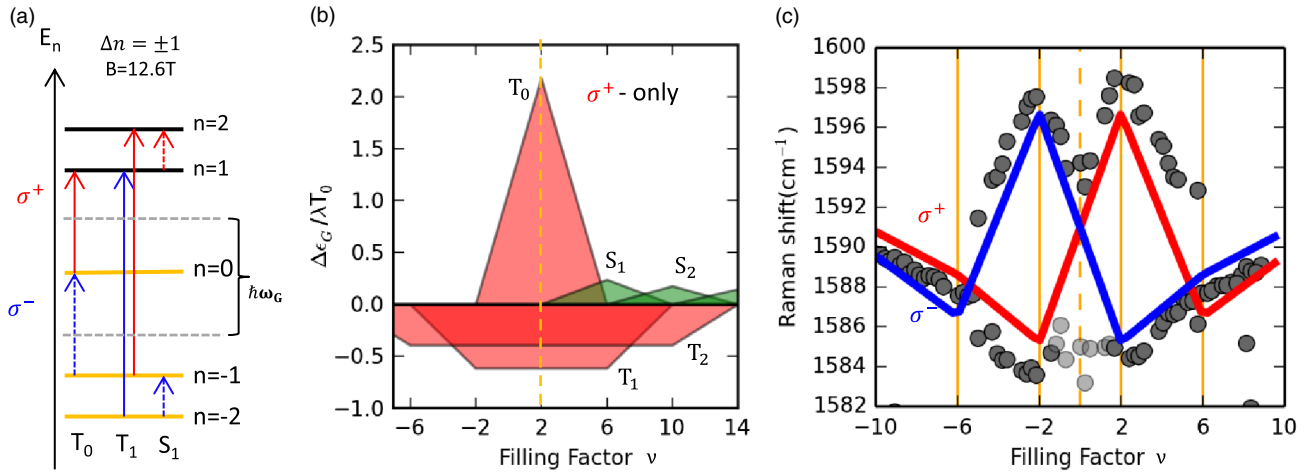

FIG. 3 (color online). (a) Schematic view of the Landau level spectrum at $B = 12.6\ T$, filling factor $\nu = 2$, and the lowest Landau level transitions participating in magnetophonon coupling. Filled electronic states are highlighted using orange color. Red and blue arrows show transitions allowed by the selection rule $\Delta|n| = \pm 1$. Dashed arrows mark Pauli blocked transitions. Circular arrows represent the angular momentum involved in the transitions. (b) Relative strength and filling factor dependence of individual terms of the phonon self-energy for σ^+-transitions. Terms describing interband transitions are shaded red, intraband transitions are shaded green. (c) Phonon energy as a function of the filling factor at $B = 12.6\ T$. Vertical orange lines mark specific filling factors at $\nu = -6, -2, 0, 2, 6$ where the $n = -1, 0, 1$ levels are completely filled or depleted with charge carriers ($\nu = 0$ corresponds to half filling of $n = 0$ level). The calculated magnetophonon energies according to Eq. (4) are plotted as solid red($\Delta n = +1$) and solid blue($\Delta n = -1$) lines. Light grey points are due to a weak asymmetry in the peak visible for low intensity (see Supplemental Material [26]).

phonon frequency ε_0 [4]. The shift of the G band in the nonresonant regime is then given by

$$\Delta\varepsilon_{\mathcal{A}} = \mathrm{Re}\left\{\lambda T_0^2\left[\sum_{n=0}^{N}\left(\frac{f_{\mathcal{A},n}(\nu)T_n}{(\varepsilon_0+i\delta)^2-T_n^2}+\frac{1}{T_n}\right)+\sum_{n=1}^{N}\frac{f_{\mathcal{A},n}(\nu)S_n}{(\varepsilon_0+i\delta)^2-S_n^2}\right]\right\}. \quad (4)$$

The expressions Eq. (3) and Eq. (4) are distinguished by the numbers of terms needed, and by their different filling factor dependence. In the resonance approximation Eq. (3) the shift is proportional to $\sqrt{\nu}$ while in the nonresonant case Eq. (4) is linear in the filling factor ν.

We now consider the effect of the charge tuning in Eq. (4) with fixed B field. In order to evaluate the contributions from participating inter- and intraband transitions, we calculate the individual contribution to the phonon energy shift $\Delta\varepsilon_n$ from each term in Eq. (4) evaluated at $B = 12.6\ T$. Shown in Fig. 3(b) are the $\Delta\varepsilon_n$ for the lowest lying inter- and intraband transitions for σ^+ polarization, i.e., transitions with $\Delta n = +1$. We use the values for ε_0, λ, v_F and δ from the $B = 0\ T$ fit. Curves are labeled as T_n (red shaded) for inter-band and S_n (green shaded) for intraband transitions, normalized by λT_0. The largest contribution is due to the T_0 term which shows a strong peak at $\nu = 2$. The contributions from the remaining inter-band transitions are strong as well. The shift due to the T_1 term is 28% and the T_2 term is still at 17.9% relative to the shift caused by the T_0 term. The action of intraband terms are restricted to a smaller range of ν values, but their strength can be significant nevertheless ($S_1/T_0 \approx 10\%$). The case of σ^- polarization is completely symmetric relative to the point $\nu = 0$.

Finally, we combine these contributions and compare to our experimental data [Fig. 3(c)]. We only include the first five terms of Eq. (4) in our calculation, since the neglected terms only cause a small overall downshift of $\sim -1\ \mathrm{cm}^{-1}$ in the range of our measurement (See Supplemental Material [26]). The phonon energy is plotted versus filling factor rather than charge density to highlight the correspondence between the filled Landau levels and the extrema of kinks in the slope (orange lines). The solid red and blue lines are the numerical results for the energies ε_{σ^+} and ε_{σ^-}. We emphasize that no adjustable parameters have been used to compare data and theory at $B = 12.6\ T$—all parameters are determined from the $B = 0$ data. The splitting between ε_{σ^+} and ε_{σ^-} is maximal at $\nu = -2$ and $\nu = 2$ where the coupling strength to the T_0 transitions with $\Delta|n| = -1$ and $\Delta|n| = +1$ are strongest. Figure 3(b) also explains the kink in slope $\nu = \pm 6$ due to Pauli blocking of T_0 and T_1 transitions. The upshift with increasing $|\nu|$ is caused by the linear decrease of the T_1 transition as the LL $n = \pm 1$ are filled or emptied, respectively. In principle, scanning the charge density to larger absolute value $|\nu|$ will reveal higher and higher n transitions by kinks in the slope, which requires high resolution in determining the peak positions. We could not resolve the small splitting of $\sim 1\ \mathrm{cm}^{-1}$ between ε_{σ^+} and ε_{σ^-} for $|\nu| > 6$ predicted by the model. Future measurements with circular polarization analysis could help determine individual ε_{σ^+} and ε_{σ^-} peak positions with higher precision. The linear model predicts zero split for the two polarizations at $\nu = 0$. The lightly shaded points in Fig. 3(c) are likely not contradictory to the model, but due to a weak asymmetry of the Raman peak, even in the absence of magnetic field (see Supplemental Material [26]). No split in the main peak can be resolved near $\nu = 0$.

By focusing on the nonresonant regime we have discovered fine structure in the G-band optical phonon in single layer graphene at high magnetic fields as a function of charge density. The observed behavior is caused by coupling between the phonon and magnetoexciton far from resonance that results in a linear dependence on filling factor, in contrast to on-resonant coupling that leads to a square root dependence on filling factor. High magnetic field Raman scattering with electrostatic tuning of the charge carrier density allows us to explore the filling factor dependent coupling strength of orthogonal, nonresonant magnetophonon states as they are being turned on and off. By including coupling to many Landau level transitions we show qualitative and quantitative agreement with numerical calculations of a linearized model of electron-phonon interactions in magnetic fields. The measured coupling strength, broadening, and Fermi velocity are in good agreement with independent observations at $B = 0\ T$ and earlier experiments.

We thank Mengkun Liu for help with sample preparation and Mark Goerbig and Alex Kitt for discussions.

*swan@bu.edu

[1] A. H. C. Neto, F. Guinea, N. M. R. Peres, K. S. Novoselov, and A. K. Geim, Rev. Mod. Phys. **81**, 109 (2009).
[2] M. O. Goerbig, Rev. Mod. Phys. **83**, 1193 (2011).
[3] M. O. Goerbig, J.-N. Fuchs, K. Kechedzhi, and V. I. Fal'ko, Phys. Rev. Lett. **99**, 087402 (2007).
[4] T. Ando, J. Phys. Soc. Jpn. **76**, 024712 (2007).
[5] S.Goler, J. Yan, V. Pellegrini, and A. Pinczuk, Solid State Commun. **152**, 1289 (2012).
[6] M. Kühne, C. Faugeras, P. Kossacki, A. A. L. Nicolet, M. Orlita, Y. I. Latyshev, and M. Potemski, Phys. Rev. B **85**, 195406 (2012).
[7] C. Faugeras, M. Amado, P. Kossacki, M. Orlita, M. Kühne, A. A. L. Nicolet, Y. I. Latyshev, and M. Potemski, Phys. Rev. Lett. **107**, 036807 (2011).
[8] J. Yan, S. Goler, T. D. Rhone, M. Han, R. He, P. Kim, V. Pellegrini, and A. Pinczuk, Phys. Rev. Lett. **105**, 227401 (2010).
[9] Y. Kim, J. M. Poumirol, A. Lombardo, N. G. Kalugin, T. Georgiou, Y. J. Kim, K. S. Novoselov, A. C. Ferrari, J.

Kono, O. Kashuba, V. I. Fal'ko, and D. Smirnov, Phys. Rev. Lett. **110**, 227402 (2013).
[10] C. Faugeras, M. Amado, P. Kossacki, M. Orlita, M. Sprinkle, C. Berger, W. A. de Heer, and M. Potemski, Phys. Rev. Lett. **103**, 186803 (2009).
[11] P. Kossacki, C. Faugeras, M. Kühne, M. Orlita, A. A. L. Nicolet, J. M. Schneider, D. M. Basko, Y. I. Latyshev, and M. Potemski, Phys. Rev. B **84**, 235138 (2011).
[12] Y. Kim, Y. Ma, A. Imambekov, N. G. Kalugin, A. Lombardo, A. C. Ferrari, J. Kono, and D. Smirnov, Phys. Rev. B **85**, 121403 (2012).
[13] P. Kossacki, C. Faugeras, M. Kühne, M. Orlita, A. Mahmood, E. Dujardin, R. R. Nair, A. K. Geim, and M. Potemski, Phys. Rev. B **86**, 205431 (2012).
[14] K. S. Novoselov, A. K. Geim, S. V. Morozov, D. Jiang, Y. Zhang, S. V. Dubonos, I. Grigorieva, and A. Firsov, Science **306**, 666 (2004).
[15] K. S. Novoselov, A. K. Geim, S. V. Morozov, D. Jiang, M. I. Katsnelson, I. V. Grigorieva, S. V. Dubonos, and A. A. Firsov, Nature (London) **438**, 197 (2005).
[16] Y. Zhang, Y.-W. Tan, H. L. Stormer, and P. Kim, Nature (London) **438**, 201 (2005).
[17] S. Pisana, M. Lazzeri, C. Casiraghi, K. Novoselov, A. Geim, A. Ferrari, and F. Mauri, Nat. Mater. **6**, 198 (2007).
[18] J. Yan, Y. Zhang, P. Kim, and A. Pinczuk, Phys. Rev. Lett. **98**, 166802 (2007).
[19] C. Stampfer, F. Molitor, D. Graf, K. Ensslin, A. Jungen, C. Hierold, and L. Wirtz, Appl. Phys. Lett. **91**, 241907 (2007).
[20] A. C. Ferrari, J. C. Meyer, V. Scardaci, C. Casiraghi, M. Lazzeri, F. Mauri, S. Piscanec, D. Jiang, K. S. Novoselov, S. Roth, and A. K. Geim, Phys. Rev. Lett. **97**, 187401 (2006).
[21] C. Casiraghi, A. Hartschuh, E. Lidorikis, H. Qian, H. Harutyunyan, T. Gokus, K. S. Novoselov, and A. C. Ferrari, Nano Lett. **7**, 2711 (2007).
[22] Z. H. Ni, H. M. Wang, J. Kasim, H. Fan, T. Yu, Y. H. Wu, Y. P. Feng, and Z. X. Shen, Nano Lett. **7**, 2758 (2007).
[23] P. Blake, E. W. Hill, A. H. C. Neto, K. S. Novoselov, D. Jiang, R. Yang, T. J. Booth, and A. K. Geim, Appl. Phys. Lett. **91**, 063124 (2007).
[24] This was presented by S. Rémi, M. Liu, A. K. Swan and B. B. Goldberg at the 2009 KIAS Graphene meeting (but not published) and cited in Refs. [9,25].
[25] T. Ando, J. Phys. Soc. Jpn. **75**, 124701 (2006).
[26] See Supplemental Material at http://link.aps.org/supplemental/10.1103/PhysRevLett.112.056803 for details of the data analysis.